Documentation of the FBH HBT Model

Matthias Rudolph

Ferdinand-Braun-Institut für Höchstfrequenztechnik (FBH),
Gustav-Kirchhoff-Str. 4, D-12489 Berlin, Germany
rudolph@fbh-berlin.de, http://www.fbh-berlin.de/modeling.html

ver 2.1.20050728

Abstract

The GaAs-HBT technology nowadays is a standard technology, which is readily available to circuit designers. However, while at least three highly accurate models for Si-based HBTs are available, good models for the GaAs and InP world are rare. In this documentation of the FBH HBT model, also the specific challenges in the modeling of these HBTs are highlighted.

Contents

1 Introduction

In recent years, heterobipolar transistors became available in commercial GaAs MMIC technology. Due to their ability to operate at high current densities they are the devices of choice for power amplifiers, e.g. in mobile phones. Also InP-based HBT technologies for high-speed circuits are available. The lower $1/f$ noise compared to HEMTs also qualifies the devices for oscillator applications. While technology is mature and industry already ships large numbers of HBT-based MMICs, the model development for circuit design lacks behind. The designer has the choice between about a dozen built-in models for GaAs-based FETs in standard circuit simulators, but models for GaAs-based HBTs are rare. This only leaves the choice to use either sophisticated models taylored for Si devices, the simple SPICE-type Gummel-Poon (GP) model, or to do the full design with a linear S-parameter based model. None of the approaches is satisfactory.

This document attempts to fill this gap. It deals with extensions of the GP model that are necessary for the description of HBTs, and eventually lead to the development of the FBH model.

Before going into details, it is necessary to point out that state-of-the-art GaAs-based HBTs are quite 'ideal' devices.

- The semi-insulating substrate prevents parasitic substrate effects that have to be accounted for on silicon.

- In a good technology, surface or interface related problems such as parasitic currents are negligible, and even thermal runaway can be supressed by proper emitter or base feedback or by thermal shunt technology.

Two effects, however, are most important to simulate HBTs. The first one is self-heating, the second is the current dependence of the transit frequency, caused by high current injection into the collector. These effects will be presented in greater detail in the following.

All exampes in this paper are measured at GaInP/GaAs HBTs fabricated on the $4''$ process line of the Ferdinand-Braun-Institut [1].

1.1 Overview over HBT Model Features

The FBH model accounts for:

- partition of intrinsic and extrinsic base-collector diode

- non-ideal base currents (Base-Emitter and Base-Collector)

- self-heating and thermal interaction (by a thermal port)

- current-dependence of base-collector capacitance and collector transit time

- base-emitter and base-collector break-down

- enhanced noise model: improved in the $1/f$ range as well as in the RF-range.

- scaling with transitor size

- unambigous analytic parameter extraction from measurements

1.2 What Kind of HBTs is the Model for?

The model is suited for GaAs-based HBTs, with AlGaAs or InGaP emitter, and for InP based HBTs and DHBTs.

It is a concentrated model that assumes an almost constant temperature allover the device. Large area devices that can not be described as concentrated elements, or those that show current crunching due to hot-spot formation can be modeled by properly interconnecting several concentrated unit cells.

Self-heating is included in the common way, treating it as an effect of low-frequency dispersion. This can cause a gap of validity of the standard model between DC and a few MHz. However, the model allows the user to define any custom thermal equivalent circuit using the thermal port.

2 Model Topology

Since substrate effects are negligible, it remains a quite simple equivalent-circuit topology as shown in Fig. 1. Due to the mesa structure of the HBTs, the total base-collector junction divides into an active part below the emitter, and a parasitic part under the base contacts. Since the current flows almost vertically from emitter to sub-collector, the parasitic part can be seen as an additional pn diode that is reverse biased in usual operation. In this document, we will refer to the part under the emitter as 'active' HBT in order to distinguish it from the parasitic BC-diode that carries no current. However, both are part of the intrinsic HBT, since the parameters are bias dependent. Only the passive embedding network is called extrinsic HBT.

In the model, the partition between active part and parasitic BC junction diode is described by a factor $XCjc$, defined as the ratio of emitter area to total BC junction area.
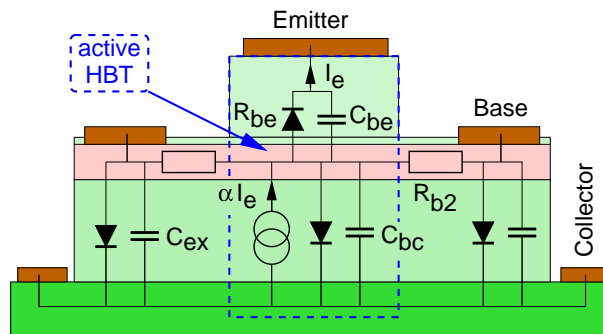
Figure 1: Schematic cross section of a single finger HBT, with intrinsic T-topology equivalent circuit. The diode symbols represent nonlinear resistors with diode characteristics.

2.1 Small-Signal Equivalent Circuit

Although this document deals with a large-signal model, it is necessary to present the small-signal equivalent circuit too. The T-topology equivalent circuit as shown in Fig. 2 is chosen for its physical significance compared to the Π-topology. Some parameters are given

3

different names so that small-signal parameters are not confused with bias dependent large-signal parameters.

Figure 2: Small-signal equivalent circuit.

The division of the total base-collector capacitance into the intrinsic and parasitic part is accounted for by the two capacitances C_{bc} (in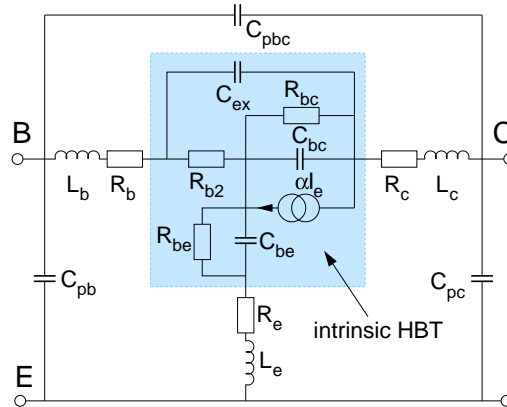trinsic active region) and C_{ex} (intrinsic parasitic). The resistance of the intrinsic part of the pn-junction is modeled by R_{bc}, while the resistance of the outer part is neglected for simplicity.

The current gain α is modeled by

$$\alpha = \frac{\alpha_0 e^{-j\omega\tau'}}{1 + j\omega/\omega_\alpha}$$

with the DC-limit of the current gain α_0 and the two time constants τ' and ω_α. The current source is driven by the total emitter current flowing through C_{be} and R_{be}.

The question of how the T-topology parameters can be transferred into Π-topology parameters is addressed in [2].

The values of the small-signal capacitances and time constants extracted in multiple bias points will be required to determine the parameters of the large signal model.

2.2   Large-Signal Equivalent Circuit

The extrinsic part of the large-signal equivalent circuit is shown in Fig. 3. It represents the passive feeding structures and contact resistances. All parameters are assumed to be independent of bias and thereby are equal to the small-signal parameters. However, the extrinsic inductances L_e, L_c, and L_b are not yet implemented in the Verilog version of the model.

The intrinsic large-signal equivalent circuit is shown in Fig. 4. Additional to the electrical part, it has a thermal subcircuit to determine the device self-heating due to dissipation of power.

In contrast to the small-signal case, the Π-topology is used here in order to keep some compatibility with the traditional Gummel-Poon model. The current source amplifies the base currents in forward and backward operation. In this topology, only the current through the resistances is amplified, as denoted in the figure. The current amplification factors are $BF = Bf - kBeta\Delta T_{j,l}$, and Br.

As in the Gummel-Poon description, the collector current is modeled by a diode-like current source, while the the base current are modeled by the same formula divided by the current gain. By doing so, the parameters determined from the Gummel-plot measurement can directly be inserted into the model.
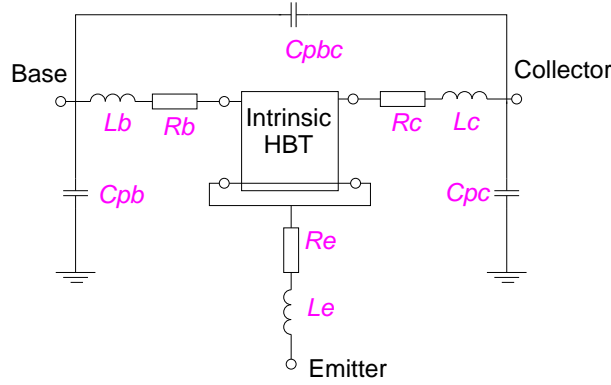
Figure 3: Extrinsic part of equivalent circuit. The element names printed in oblique magenta letters are also names of model parameters.
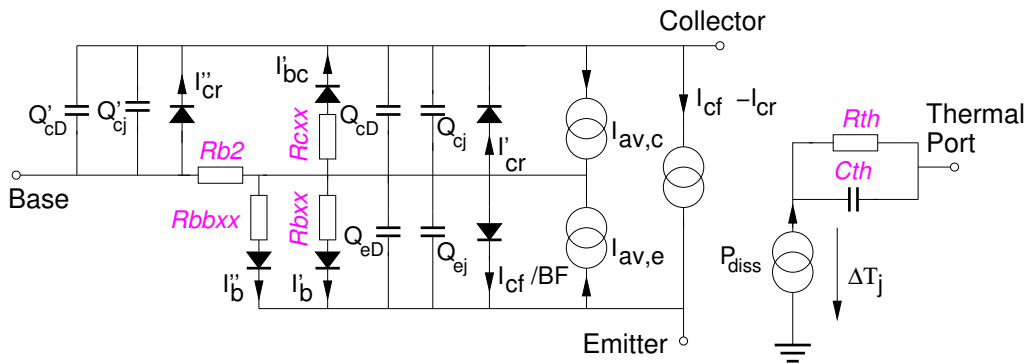

Figure 4: Intrinsic part of large-signal equivalent circuit. The element names printed in oblique magenta letters are also names of model parameters.

The diode symbols represent bias dependent resistances with diode characteristics. In forward operation case, the collector current is modeled by the current source. The current I_{cf}/BF represents the ideal base-emitter current that is amplified. The currents I'_b, I''_b, and I'_{bc} represent the nonideal (parasitic) base currents. The bias independent resistors $Rbxx$, $Rbbxx$, and $Rcxx$ are included to model the possible saturation of these current components. The base-collector current is split into two components due to the mesa structure of the HBT: the current I'_{cr} inside the active HBT, and the parasitic current I''_{cr}. The currents are derived from I_{cr} using the partition factor $XCjc$. In case of equal voltages, $I'_{cr} = XCjc \cdot I_{cr}/Br$, and $I''_{cr} = (1 - XCjc) \cdot I_{cr}/Br$. However, I'_{cr} is driven by the intrinsic base-collector voltage, while I''_{cr} is driven by the voltage across the parasitic part of the diode. Both diodes are divided by the resistance of the intrinsic base layer $Rb2$ which is assumed to be constant as a first order approximation.

Base-collector and base-emitter break-down is modeled by two current sources $I_{\mathrm{av,c}}$ and $I_{\mathrm{av,e}}$.

The large-signal model contains bias dependent charge sources which for convenience in the figure are drawn as their small-signal equivalents, capacitances. Two charges are shown for both junctions, a diffusion (Q_{xD}) and a depletion (Q_{xj}) capacitance.

A current equivalent to the total dissipated power P_{diss} is fed to a thermal subcircuit. The voltage ΔT_j then equals the temperature rise due to self-heating of the device.

Note Parameters such as Lb or Rth (written in magenta) that also describe elements of the equivalent circuit (in contrast to those that are only parameters used in a formula) will

5

be written in the following with indices as L_b and R_{th} for better readability.

3   DC and Self-Heating Model

3.1   Thermal Subcircuit

The temperature rise due to self-heating, ΔT_j, is determined from an equivalent voltage across the thermal subcircuit shown in Fig. 4. The dissipated power P_{diss} is approximately converted into an equivalent current and fed to the thermal subcircuit:

$$P_{\mathrm{diss}} = I_{\mathrm{cf}} \cdot v_{\mathrm{ce}} + I_{\mathrm{cf}}/B_F \cdot v_{\mathrm{be}} + I_{\mathrm{cr}} \cdot v_{\mathrm{ce}} + I_{\mathrm{cr}}' \cdot v_{\mathrm{cb}} + I_{\mathrm{cr}}'' \cdot v_{\mathrm{cbx}} \tag{1}$$

The dissipated power is determined with the intrinsic voltages v_{be}, v_{ce}, and v_{bc}. It is assumed that the HBT self-heating takes place under active forward operation, and that the contribution of parasitic currents and voltages do not contribute significantly.

An additional thermal port is provided to allow the modeling of mutual heating of individual lumped elements or dynamic changes in ambient temperature. Those changes can be accounted for by applying an equivalent voltage to the thermal port. Setting the parameter R_{th} to zero allows to apply an arbitrary external thermal subcircuit. If no such feature is needed, the thermal port is set to ground.

A parameter $Temp$ is defined for the ambient temperature. This parameter is used to determine the actual temperature together with self-heating (also to determine the thermal noise). The junction temperature thereby is given by $T_j = Temp + \Delta T_j$.

A parameter $Tnom$ is defined for the reference temperature at which the parameters have been extracted. Some parameters, e.g. the forward current gain, are modeled linearly dependent on temperature. The parameter change then has to take into account the difference of the junction temperature with respect to the nominal temperature: $\Delta T_{j,l} = (Temp + \Delta T_j) - Tnom$.

3.2   Thermal DC Model

Since HBTs are operated usually at high power densities, self-heating plays an important role. Temperature affects the electrical behaviour of an HBT mainly in two ways:

- The current gain β decreases almost linearly with increasing temperature. This leads to a decreasing I_C in an output IV plot with I_B held constant as a parameter (see Fig. 5).

- At constant I_B, V_{BE} decreases linearly as temperature is increased, which also can be seen in the measured Gummel plot in Fig. 6. This is caused by the exponential dependence of the base-emitter diode's current on both voltage and temperature.

The temperature-dependent equation for a diode DC current is given by[1]:

$$I = I_s e^{V_g/V_{th,0} - V_g/V_{th}} \left(e^{V_{be}/(nV_{th})} - 1 \right) \tag{2}$$

 with the saturation current I_s, an activation energy $E_g = V_g/q$, the thermal voltage at junction temperature V_{th} and that at a reference temperature $V_{th,0}$, and the ideality factor n.

In order to suppress numerical instabilities due to (false) inverse thermal runaway as described in [3], the diode currents are limited in reverse bias. The reverse current may

---

[1]A factor that sets the temperature to a power was omitted in the formula for simplicity due to its reduced importance compared to the exponential term.

not exceed its value at Tnom by a factor higher than 10^6. This bound should not affect the accuracy in normal operation.

The model parameters are:

	in Fig. 4	I_s	n	E_g
ideal forward collector current	I_{cf}	J_{sf}	n_f	V_{g}
total reverse collector current	I_{cr}	J_{sr}	n_r	V_{gr}
parasitic BE current	I'_b	J_{se}	n_e	V_{gb}
2. parasitic BE current	I''_b	J_{see}	n_{ee}	V_{gbb}
parasitic BC current	I'_{bc}	J_{sc}	n_{c}	V_{gc}

The parasitic base current diodes may be switched off by setting (J_{se} or n_e), (J_{see} or n_{ee}), or (J_{sc} or n_c) to zero.

The parasitic base currents are used to account for different slopes of base and collector current, as seen in the Gummel plot in Fig. 6. These currents are due to recombination at the interface or at the base surface and are not amplified. Since it often is observed that these current components saturates at higher forward voltages (The parasitic currents usually are not present in useful bias points), saturation resistances R_{bxx}, R_{bbxx}, and R_{cxx} are implemented in series.

The forward current gain β is modeled to depend linearly on temperature:

$$B_F = B_f - k_{\mathrm{Beta}} \cdot \Delta T_{j,l} \tag{3}$$

while the reverse current gain B_r is kept constant.

It is necessary to prevent B_F from changing its sign at non-physically high temperatures. A hard-limit is used that keeps B_F at a constant value of 10^{-6} instead of decreasing further.
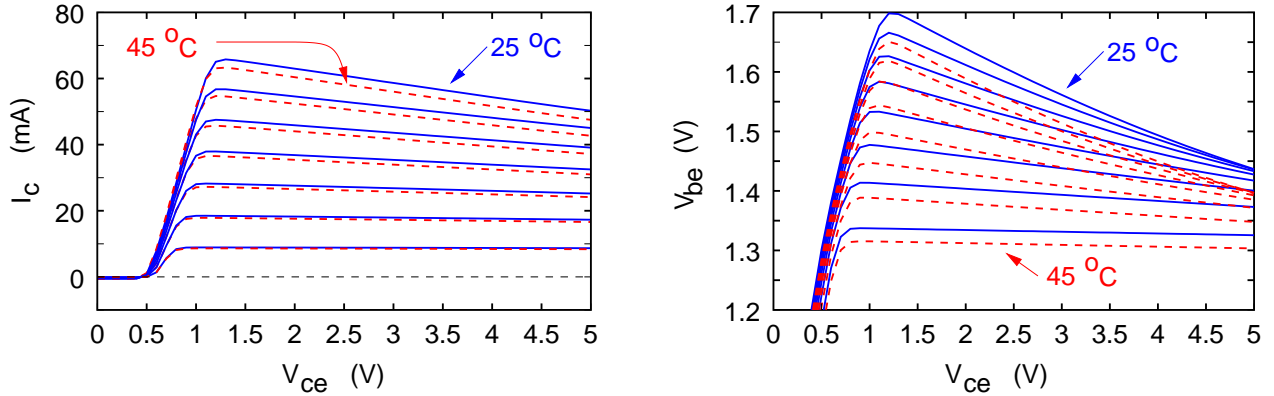

Figure 5: Output IV curves of HBT with constant I_B at ambient temperatures of $25°$ C and $45°$ C.

3.3 Thermal Capacitance

Although the thermal capacitance is not a real DC parameter, it is discussed here together with R_{th} . While a negative differential resistance effect is seen in output IV-curves, no such effect occurs in the microwave region. Thermal time constants of about $1\,\mu$s are reported in the literature. Therefore, it is possible to use C_{th} only to decouple the DC bias point (which defines the actual temperature) and the RF frequencies (which do not). Fig. 7 shows a S-measurement down to the kHz range, where it clearly can be seen that thermal effects lead to a strange behaviour. Also $|S_{22}| > 1$ can be observed. However, this frequency range is out of the scope of this model. Every frequency beyond DC is simulated isothermal — at a
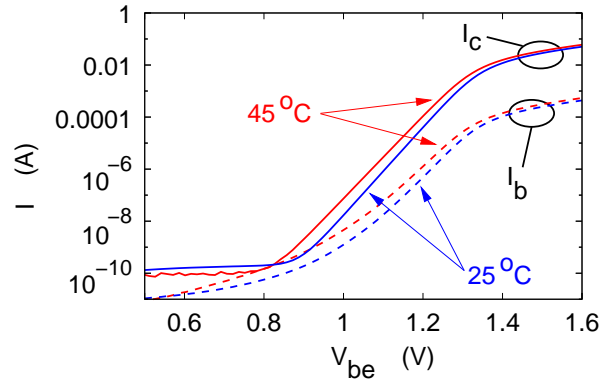
Figure 6: Gummel plot of HBT at ambient temperatures of $25°$ C and $45°$ C.

temperature defined by the ambient temperature parameter $Temp$, the thermal resistance R_{th} and the dissipated DC power. If a more sophisticated model for thermal dissipation with multiple time constants is needed, an appropriate filter can be applied to the thermal port. The simple built-in thermal model then can be switched off by setting R_{th} to zero.
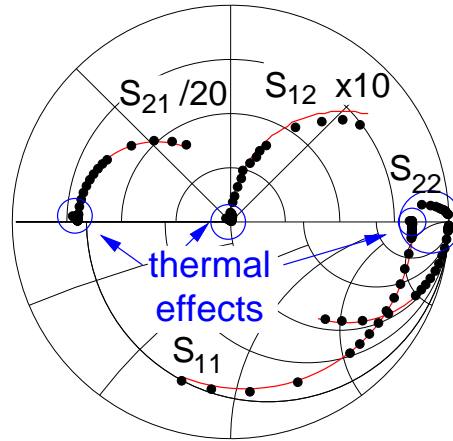
Figure 7: S-parameters of a $3{\times}30\,\mu$m^2 HBT, measured and simulated, I_c= 30 mA, V_{ce}=3 V, $f = 300$ kHz … 3 GHz.

Note   Additionally to the DC parameters discussed so far, temperature has an impact on the base transit time, that increases proportionally with temperature. This will be discussed later on in the section on transit times and capacitances. The temperature dependence of the other parameters, such as the extrinsic resistances, can be neglected without significantly affecting accuracy.

3.4   Early and Webster Effects

As in the Gummel-Poon model, the impact of these two effects is described by modification of the normalized base charge q_b. The individual functions are borrowed from the VBIC model, with

$$q_b = \frac{q_1 + \sqrt{q_1^2 + 4\,q_2}}{2} \tag{4}$$

The normalized charge reduces the base-emitter current:

8

$$I_{\text{cf}} - I_{\text{cr}} = \frac{I'_{\text{cf}} - I'_{\text{cr}}}{q_b} \tag{5}$$

With the ideal currents in absence of Webster and Early effects are denoted by I'_{cf} and I'_{cr}.

3.4.1   Early Effect

Although the Early effect generally is of minor importance in HBTs due to the high base doping, it might be necessary to account for it in special cases. Therefore the normalized charge q_1 is defined:

$$q_1 = 1 + \frac{Q_c(V_{bc}) - Q_c(0)}{C_{jc} \cdot \text{VAF}} + \frac{Q_{je}(V_{be}) - Q_{je}(0)}{C_{je} \cdot \text{VAR}} \tag{6}$$

Where $Q_c(V_{bc})/C_{jc}$ and $Q_{je}(V_{be})/C_{je}$ denote the normalized charge of the base-collector and base-emitter space-charge regions, as defined in 4.3.1. Setting VAR or VAF to zero switches the Early effect off for the respective junction.

3.4.2   Webster Effect

High current injection into the base normally is not observed in HBTs due to the high base doping. However, the VBIC description for the effect is used, and it is described by two parameters IKF and IKR:

$$q_2 = \frac{I'_{\text{cf}}}{A_e \cdot \text{IKF}} + \frac{I'_{\text{cr}}}{A_e \cdot \text{IKR}} \tag{7}$$

3.5   Break-Down

Break-down is modeled for base-emitter and base-collector junctions. The break-down is modeled in different ways for the two junctions.

3.5.1   Base-Emitter Break-Down

Base-emitter break-down occurs when the base-emitter voltage exceeds a certain limit. Since it it assumed that the HBT is in forward active mode, approximately no emitter current flows at negative V_{be} values in absence of break-down.

The emitter current due to break-down is modeled similar to the SPICE diode break-down model by the current source $I_{\text{av,e}}$ in parallel with the base-emitter pn-junction (see Fig. 4):

$$I_{\text{ac,e}} = J_{\text{sf}} e^{-(BV_{\text{BEO}} + V_{be})/V_{\text{th}}} \tag{8}$$

with the base-emitter break-down voltage BV_{BEO}.

Setting BV_{BEO} to zero switches the BE break-down model off.

3.5.2   Base-Collector Break-Down

In case of the base-collector break-down, it is assumed that the collector current is increased by multiplication. The multiplication factor is defined by:

$$M(V_{bc}) = \frac{1}{1 - (-V_{bc}/BV_{\text{CEO}})^{M_c}} \tag{9}$$

Thereby the breakdown current $I_{\text{av,c}}$ becomes:

$$I_{\text{av,c}} = K_c \cdot (M - 1) \cdot I_{\text{cf}} \tag{10}$$

9

Setting one of the parameters to zero switches the break-down model off for the BC junction.

For zero reverse voltages or forward bias, the factor M is fixed to unity:

$$M(V_{bc}) = 1 \qquad \Rightarrow I_{\mathrm{av,c}} = 0 \qquad \text{for } V_{bc} \geq 0$$

Linear approximation of M is used to cope with the singularity at $V_{bc} = BV_{\mathrm{CEO}}$, similar to the junction capacitance formulation. A factor $FBD = V_{bc,x}/BV_{\mathrm{CEO}}$ defines the onset of the linear part at a voltage $V_{bc,x}$ relative to BV_{CEO}.

$$M(V) = \frac{1}{1 - FBD^{M_c}} - \frac{M_c}{BV_{\mathrm{CEO}}} \cdot \frac{FBD^{M_c-1}}{(1 - FBD^{M_c})^2} \cdot (FBD \cdot BV_{\mathrm{CEO}} + V_{bc}) \qquad \text{for } V_{bc} \leq -FBD \cdot BV_{\mathrm{CEO}}$$

(11)

4 Capacitance and Transit-Time Effects

4.1 Basic Concept

As shown in Fig. 4, each of the pn-junctions is modeled with two components: depletion and diffusion capacitances. All capacitances are implemented as charges.

Transit-time components are also modeled using charges. Three types of transit times have to be accounted for: base-emitter charging time τ_{be}, and base and collector transit times, τ_b and τ_c, respectively. The time constants present in the small-signal case, Fig. 2, are commonly modeled by:

$$\alpha = \frac{\alpha_0 e^{j\omega\tau'}}{1 + j\omega/\omega_\alpha}$$

(12)

The question is, how to approximate this formula in an equivalent circuit with a frequency independent current source α_0 and no time delay.

The idea of the implementation is best explained looking at the T-topology equivalent circuit of the active HBT, Fig. 8. In the figure, the charge sources Q_e and Q_c represent all capacitive contributions at base-emitter and base-collector junction.

Emitter charging time and base transit time is modeled as in the GP model, simply by redefinition of the driving current. While in Fig. 2, the total emitter current I_e is amplified, in Fig. 8, only the emitter current I'_e is amplified. This modifies the effective current gain, since the time constant of the base-emitter junction gains influence:

$$\alpha_0 I'_e = \frac{\alpha_0}{1 + j\omega(\tau_{be} + \tau_b)} I_e$$

(13)

with $(\tau_{be} + \tau_b) = C_{be}R_{be}$. This formula is a first-order approximation of the desired exponential description of eq. (12). In order to account for the time constants, it thereby is necessary to properly adjust the capacitive elements of the base-emitter junction: τ_{be} is modeled using the depletion capacitance, while τ_b is modeled using a diffusion capacitance description.

Concerning τ_c, a transcapacitance approach is implemented.[2] This links transit-time and capacitance effects in the depleted collector region together in a physically meaningful way. An appropriate function for the collector charge Q_c is to be found. By definition, the derivative of Q_c with respect to V_{bc} yields the capacitance. The impact on τ is not as obvious.

Q_c, as shown in Fig. 8 is a function of V_{be} and V_{bc}. In the small-signal case, Fig. 9, Q_c yields two elements: C_{bc} and the transcapacitance $C_{tr} = \partial Q_c/\partial V_{be}$. The latter can be

---

[2]A transcapacitance implementation has already been proposed to model the HBT's base transit-time [4], and is the underlying idea in the "charge partitioning" approach [5].
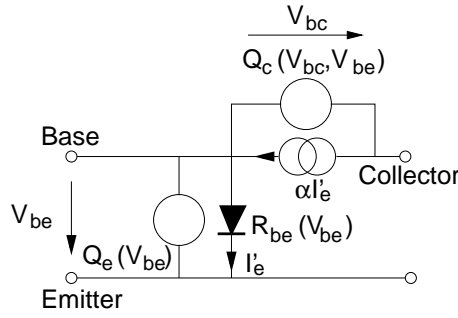
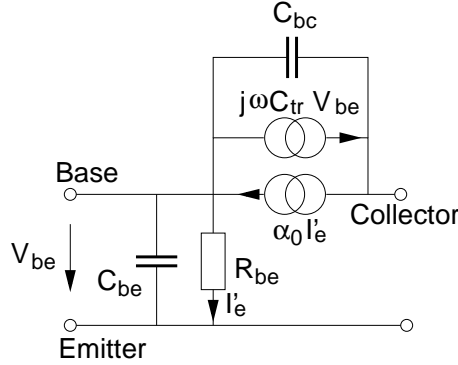Figure 8: Part of the large-signal equivalent circuit.

Figure 9: Part of the small-signal equivalent circuit derived from Fig. 8.

understood as a current source that is driven by the base-emitter voltage V_{be}. Since they are in parallel, the current source α and the transcapacitance can be added:

$$
\begin{aligned}
\alpha' I_e' &= \alpha_0 I_e' - j\omega C_{tr} V_{be} \\
&= (\alpha_0 - j\omega C_{tr} R_{be}) I_e'
\end{aligned}
\tag{14}
$$

with $C_{tr} R_{be} = \tau_c$. If we now define the total emitter current I_e (see Fig. 1, and eq. (13)) as the driving current instead of only the current I_e' through R_{be}, we end up with

$$
\alpha = \frac{\alpha_0 - j\omega\tau_c}{1 + j\omega(\tau_{be} + \tau_b)}
\tag{15}
$$

This implementation has been proven to yield accurate results up to the transit frequency [2, 10]. It furthermore is possible to account for velocity modulation effects and base push out in a unified way.

4.2 Differences to Si Devices

Looking at the bias dependence of the transit frequency f_t of InP and GaAs HBTs, some differences to the GP model can be seen.

In the GP model, f_t is dominated by the base-emitter charging time τ_{be} at low currents. The charging time is given by the base-emitter resistance R_{be} and the base-emitter capacitance C_{be}, and is inversely proportional to the emitter current I_e. At sufficiently high currents, f_t is dominated by the base transit time τ_b, which is fairly constant if Early effect can be neglected. Finally, at high current injection into the collector, f_t rapidly decreases due to Kirk effect (base push-out) [6].

Concerning III-V HBTs, the picture is different for medium currents. As shown in Fig. 10 for a GaAs-HBT, a region of more-or-less constant f_t cannot be seen. In contrast, one or

11

two kinks (marked 1 and 2) sometimes appear near the current where the emitter charging time becomes negligible. But f_t increases monotonically until base push-out sets in (point marked 3) and the RF performance degrades.

This behaviour can be studied regarding the total time-delay τ of the current source α of the small-signal equivalent circuit. The investigation presented in this section is based on small-signal equivalent circuit parameters [2] in order to gain insight into the individual contribution of the intrinsic elements to the over-all RF behaviour. In contrast to the external transit time $\tau_{\mathrm{ext}} = 1/(2\pi f_t)$, the intrinsic transit time τ is only given by τ_b, collector transit time τ_c, and τ_{be}, and can be approximated from the following empirical formula for α:

$$\alpha = \frac{\alpha_0 e^{j\omega\tau'}}{1 + j\omega/\omega_\alpha} \approx \frac{\alpha_0}{1 + j\omega\tau} \tag{16}$$
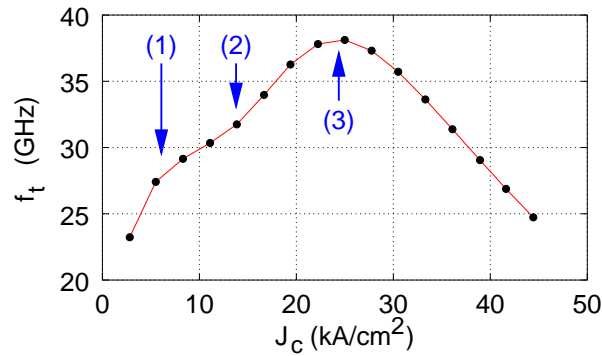
Figure 10: Typical current dependence of transit frequency ($3 \times 30\,\mu m^2$ HBT at $V_{CE} = 2\,V$).

This quantity is shown in Fig. 11 for different collector-emitter voltages V_{CE}. A strong dependence on V_{CE} is observed, since τ increases with the base-collector reverse bias voltage. The graph also shows the part of τ that is caused by the ideal constant τ_b and current-dependent τ_{be}. It is obvious from this figure, that neither the voltage dependence nor the current dependence can be modeled in the traditional way. The collector transit time τ_c plays an important role. In the following, we will first focus on current densities below the onset of base push-out, that sets in at the current marked (3) in Fig. 10.

4.3 Current Densities Below Base Push-Out

Figure 11: Typical bias dependence of intrinsic transit time. Shown is the total transit time τ, and the parts caused by base and base-emitter junction, τ_b and τ_{be}. Symbols: extracted values, lines: model ($3 \times 30\,\mu m^2$ HBT, $V_{CE} = 1.5\,V \ldots 5\,V$).

12

Figure 12: Typical bias dependence of C_{bc}, symbols: extracted values, red curve: linear current dependent model ($3 \times 30\,\mu m^2$ HBT, $V_{CE} = 1.5\,V \ldots 5\,V$).
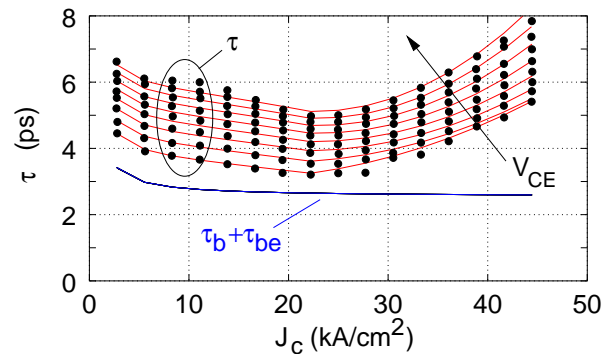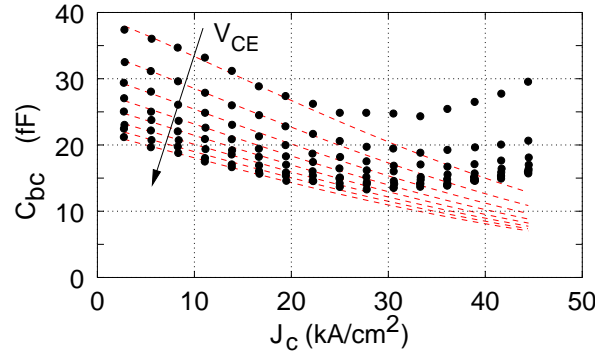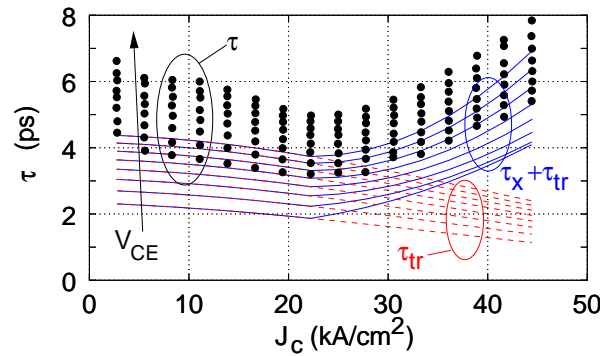

Figure 13: Typical bias dependence of τ, symbols: extracted values, red curve: collector transit time due to linear current dependence of charge, blue: collector transit time and excess transit time including to base push-out model ($3 \times 30\,\mu m^2$ HBT, $V_{CE} = 1.5\,V \ldots 5\,V$).

Since the presence of electrons in the base-collector space-charge region obviously can not be neglected, we have to take into account that they will affect the charge Q_{cj} stored there. The charge will be increased by an additional term $- \int \tau_c dI_c$, since the electrons of the collector current remain in the space charge region for some time given by τ_c. However, τ_c is not the only parameter related to Q_{cj}: the base-collector capacitance $C_{bc} = \partial Q_{cj}/\partial V_{bc}$ will also depend on current. Both small-signal quantities, τ_c and C_{bc}, therefore have to be derived from a common charge Q_{cj} and are not independent of each other. Before further stressing the interrelation of those parameters, we will have a look at the bias dependence of C_{bc}.

Fig. 12 shows the intrinsic base-collector capacitance extracted from measurements. Shown here is C_{bc}, the part of the BC capacitance that is located vertically below the emitter which is affected by the current. A fairly linear dependence is observed until base push-out sets in [8, 9].

The physics behind the bias dependence observed in τ_c and C_{bc} is quite complicate. For example, the charge of the electrons will compensate the doping in the collector and finally effectively reverse the polarity of the material, which results in base push-out [6]. This affects the width of the space-charge region. However, also other effects may take place in the collector: velocity overshoot, or an increased velocity due to a reduced field at high currents. With other words: the current modulates the electron velocity by modulating the electric field.

In case of GaAs HBTs, e.g. the behavior shown in Figs. 11, and 12 is typical and can be modeled by relatively simple analytic expressions. This also holds for InP HBTs and

13

DHBTs.

In order to account for these effects in a large-signal model, it is necessary to find the nonlinear charges and current sources that yield the desired small-signal behaviour when linearized at a certain bias point.

The following formula for Q_{cj} is found to be suited up to the onset of base push-out:

$$Q_{cj} = X_{\text{cjc}} \left[1 - \tanh\left(\frac{I_c}{I_0}\right) \right] \cdot \left[Q'_c(V_{bc}) + (1 - X_{\text{J0}})\, C_{\min} V_{bc} \right] + X_{\text{cjc}} X_{\text{J0}}\, C_{\min} V_{bc} \qquad (17)$$

Where the current $I_c = I_0$ is defined as the point were Q_{jc} would reach the minimum value for purely linear function. The minimum value of the BC capacitance can be reduced by a factor of X_{J0} compared to the value $C_{\min}$ at zero current.

For the exact formula of the space-charge capacitance $Q'_c(V_{bc})$ see below. The dashed red curves in Figs. 12 and 13 show the intrinsic capacitance and the part of τ_c (called τ_{tr}) that results from this formula.

This description has been found to be accurate even beyond the transit frequency. It has mainly two advantages. First, we can account for time-delay effects without the need to access previous time-steps in the nonlinear description. Some simulators have problems with that. The resulting formula for Q_c also is relatively simple, while it describes two effects at a time. Second, the extraction of the parameters necessary for the model is easily and analytically done from the current dependence of C_{bc}. The only parameters that are to be determined in addition to the common junction capacitance parameters: a minimum capacitance $C_{\min}$, the factor X_{J0}, and the collector current I_0, where the minimum capacitance would be reached for a linear function instead of the tanh.

The parasitic base-collector capacitance is not modulated by collector current, and therefore is modeled by:

$$Q'_{cj} = (1 - X_{\text{cjc}}) \left[Q'_c(V_{bc,\text{ex}}) + C_{\min} V_{bc,\text{ex}} \right], \qquad (18)$$

The diffusion capacitances are modeled by:

$$Q_{eD} = (T_{\text{f}} + T_{\text{ft}} \cdot \Delta T_{j,l}) I_{\text{cf}} \qquad (19)$$

$$Q_{cD} = T_{\text{r}} I_{\text{cr}} \qquad (20)$$

$$Q'_{cD} = T_{\text{rx}} I''_{\text{cr}} \qquad (21)$$

T_{ft} accounts for the temperature dependence of the base transit time.

4.3.1   Depletion capacitance description

The formula describing the depletion capacitances follows the description used in the MEX-TRAM model. Detailed information is found in [7].

In order to get rid of the pole in the charge function at the diffusion voltage, the voltage V is replaced by a limited voltage V_j:

$$V_j(V) = \begin{cases} V - V_{\text{ch}} \log\left(1 + e^{(V-VF)/V_{\text{ch}}}\right) & \text{for } V < VF \\[2mm] VF - V_{\text{ch}} \log\left(1 + e^{(VF-V)/V_{\text{ch}}}\right) & \text{for } V > VF \end{cases} \qquad (22)$$

$$Q = A_e\, C_0 \left\{ \frac{V_d}{1-m} \cdot \left[\left(1 - \frac{V_{jo}}{V_d}\right)^{1-m} - \left(1 - \frac{V_j}{V_d}\right)^{1-m} \right] + \frac{V - V_j + V_{jo}}{(1 - VF/V_d)^m} - \frac{V_d}{1-m} \right\} \qquad (23)$$

With $V_{jo} = V_j(V = 0)$, the emitter area A_e, the junction capacitance at $V = 0$ C_0, the junction grading coefficient m, the diffusion voltage V_d, and a transition parameter VF, which is fixed in the model to $VF = 0.9\, V_d$ for simplicity. The difference of this equation

compared to the original MEXTRAM description is the scaling with A_e, and the term $-\frac{V_d}{1-m}$ that is introduced to obtain the same charge value at $V = 0$ as with the idealized function.

The following parameters are required to describe the base-emitter and base-collector space-charge capacitances:

Charge	C_0	m	V_d
Q'_c	$(C_{\mathrm{jc}} - C_{\mathrm{min}})$	m_{jc}	V_{jc}
Q_{ej}	C_{je}	m_{je}	V_{je}

4.4   Current Densities Beyond Base Push-Out

In this version, the transit-times under base push-out condition are modeled according to the HICUM description [18].

However, some of the parameters are redefined. Current density J_{ck} at which the base push-out sets in is defined by the parameters R_{ci0}, R_{Jk}, and J_{k}. At low voltages, the asymptote defining J_{ck} is given by $1/R_{\mathrm{ci0}}$. At higher voltages, the asymptote is defined by $J_{\mathrm{k}} + V_{cb}/R_{\mathrm{Jk}}$ The parameters Vlim and Vpt defined in [18] can be obtained by:

$$\mathrm{Vlim} \quad = \quad \frac{J_{\mathrm{k}} R_{\mathrm{ci0}}}{1 - R_{\mathrm{ci0}}/R_{\mathrm{Jk}}} \tag{24}$$

$$\frac{1}{\mathrm{Vpt}} \quad = \quad \frac{1 - R_{\mathrm{ci0}}/R_{\mathrm{Jk}}}{R_{\mathrm{Jk}} J_{\mathrm{k}}} \tag{25}$$

5   Parameter Scaling

Scaling is provided in the FBH model to account for different layouts of HBTs in a circuit. However, in order to keep the model simple, it is assumed that the HBTs are defined by a common basic single-emitter cell. All resistances are thereby given as a function of the number of emitter fingers N, while currents and pn-junction properties are defined as functions of the total emitter area $A_e = N \times (L \times W)$. This area for simplicity also applies to the base-collector diode. No scaling is performed with extrinsic reactances, for they model the feeding structure and thereby heavily depend on layout.

The idea behind that is to simplify parameter extraction in three ways:

- extrapolation of the set of parameters once obtained to a different size (verification and fine-tuning required, but no full extraction),

- interpolation between HBTs of different size that are known to be modeled well (even for HBTs that are not fabricated yet), and

- extract a parameter from a type of HBT where it is easier (e.g. resistances are better obtained from single-finger HBTs even if one is only interested in large power cells).

The scaled model parameters are:

	parameters		
A_e	Diode currents	[A/μm^2]	J_{sf}, J_{se}, J_{see}, J_{sr}
	current limits	[A/μm^2]	J_k, J_0
	zero-voltage capacitances	[F/μm^2]	C_{je}, C_{jc}
	minimum capacitance	[F/μm^2]	C_{min}
N	extrinsic resistances	[Ω/finger]	R_e, R_b, R_c
	intrinsic resistances	[Ω/finger]	R_{bxx}, R_{bbxx}, R_{b2}

Verification of the scaling approach and detailed description is published in [8, 11, 12].

15

6 Noise Model

6.1 White Noise

All resistances – intrinsic and extrinsic – exhibit thermal noise at the actual internal temperature. By setting the parameter Noise=False, the noise model is switched off and HBT becomes noise-free.

Shot noise is included by two noise sources according to [13]. The base-emitter shot-noise current is driven by $I_b = I_{\rm cf}/B_F$, the collector-emitter shot-noise current is driven by $I_{\rm cf}$. The correlation time constant τ_n is approximated by:

$$\tau_n = (T_{\rm f} + T_{\rm ft} \cdot \Delta T_{j,l}) + \frac{\partial Q_{eD,x}/\partial V_{be}}{\partial I_{\rm cf}/\partial V_{be}} = \tau_b$$

The shot noise sources thereby become:

$$
\begin{aligned}
\langle|{\rm i}_b|^2\rangle &= 2eB\left(I_b + \left|1 - e^{-j\omega\tau_n}\right|^2 I_{\rm cf}\right) \\
\langle|{\rm i}_c|^2\rangle &= 2eBI_{\rm cf} \\
\langle{\rm i}_b{\rm i}_c^*\rangle &= 2eB\left(e^{j\omega\tau_n} - 1\right)I_{\rm cf}
\end{aligned}
\tag{26}
$$

With $I_b = I_{\rm cf}/B_F$ in Fig. 4. Since the noise sources are fully determined by temperature, resistances, currents and transit-times, no additional parameter is needed to model the RF noise.

6.2 Low-Frequency Noise

The low-frequency noise model has two noise sources [14]. The first one is the well-known noise-current source in parallel with the base-emitter junction, defined by the power current spectrum:

$$S_{Ib} = K_{\rm fb}\frac{I_b^{A_{\rm fb}}}{f^{F_{\rm feb}}} + K_{\rm b}\frac{I_b^{A_{\rm b}}}{1 + (f/F_{\rm b})^2} \tag{27}$$

If $F_{\rm b} = 0$, the Lorentz-type part of the spectrum is switched off and the equation simplifies to

$$S_{Ib} = K_{\rm fb}\frac{I_b^{A_{\rm fb}}}{f^{F_{\rm feb}}} \tag{28}$$

This source is also implemented into standard GP models. However, it turned out that it is necessary to include a second noise source to model the contribution of the bulk emitter. Its voltage spectrum is defined as:

$$S_{Ve} = K_{\rm fe}\frac{I_b^{A_{\rm fe}}}{f^{F_{\rm fee}}} \tag{29}$$

In order to circumvent problems at DC ($f \to 0$), S_{Ib} the frequency is not allowed to drop below $\omega = 1\,s^{-1}$.

7   Summary of Model Parameters

	Geometrical Parameters		
N	number of emitter fingers	number	
L	length of an emitter finger	[m]	
W	width of an emitter finger	[m]	
	General Model Settings		
Temp	ambient temperature	[°C]	see p. 6
Tnom	reference temperature at which the model parameters were extracted	[°C]	see p. 6
Mode	obsolete (ignored)		
Noise	switches noise model on or off	(0|1) or (False|True)	
Debug	ignored	(0|1)	
DebugPlus	ignored	(0|1)	
	Thermal Subcircuit		
Rth	thermal resistance	[K/W]	see p. 6
Cth	thermal capacitance		see p. 7
	Diode (DC) Parameters		
Jsf	ideal forward collector saturation current	[A/μm^2]	see p. 7
nf	ideal forward collector current ideality factor		see p. 7
Vg	ideal forward collector current thermal activation voltage	[V]	see p. 7
Jse	parasitic base-collector saturation current	[A/μm^2]	see p. 7
ne	parasitic base-collector current ideality factor		see p. 7
Rbxx	saturation resistance of non-ideal BC current	[Ω/finger]	see p. 5
Vgb	parasitic base-emitter current thermal activation voltage	[V]	see p. 7
Jsee	2. parasitic base-emitter saturation current	[A/μm^2]	see p. 7
nee	2. parasitic base-emitter current ideality factor		see p. 7
Rbbxx	2. saturation resistance of non-ideal BE current	[Ω/finger]	see p. 5
Vgbb	2. parasitic base-emitter current thermal activation voltage	[V]	see p. 7
Jsr	ideal reverse collector saturation current	[A/μm^2]	see p. 7
nr	ideal reverse collector current ideality factor		see p. 7
Vgr	ideal reverse collector current thermal activation voltage	[V]	see p. 7
XCjc	ratio of emitter to base-collector junction areas	(0,1)	see p. 3
Jsc	parasitic base-collector saturation current	[A/μm^2]	see p. 7
nc	parasitic base-collector current ideality factor		see p. 7
Rcxx	saturation resistance of non-ideal BC current	[Ω/finger]	see p. 5
Vgc	parasitic base-collector current thermal activation voltage	[V]	see p. 7
Bf	forward current gain at reference temperature		see p. 7
kBeta	(negative) slope of forward current gain with temperature		see p. 7
Br	reverse current gain		see p. 7
VAF	forward early voltage	[V]	see p. 9
VAR	reverse early voltage	[V]	see p. 9
IKF	forward high-injection knee current	[A/μm^2]	see p. 9
IKR	reverse high-injection knee current	[A/μm^2]	see p. 9
	Break-Down Parameters		

17

Mc	C-E breakdown exponent		see p. 9
BVceo	C-E breakdown voltage	[V]	see p. 9
kc	C-E breakdown factor		see p. 9
BVebo	E-B breakdown voltage	[V]	see p. 9
	Capacitances and Time Constants		
Tr	time-constant of intrinsic base-collector diffusion capacitance	[s]	see p. 14
Trx	time-constant of extrinsic base-collector diffusion capacitance	[s]	see p. 14
Tf	time-constant of base-emitter diffusion capacitance	[s]	see p. 14
Tft	temperature parameter of Tf		see p. 14
Ahc	smoothing parameter for J_{ck} (onset of base push-out)		see [18]
Thcs	saturation storage time (base push-out)		see [18]
Jk	collector current, onset of base push-out $V_{bc} = 0$	[A/μm^2]	see p. 15
RJk	slope of onset of base push-out with V_{cb}	[Ω]	see [18]
Rci0	low voltage slope of onset of base push-out with V_{cb}	[Ω]	see [18]
Vces	voltage shift for onset of base push-out	[V]	see [18]
J0	collector current at which C_{bc} reaches C_{min}	[A/μm^2]	see p. 14
Cje	B-E depletion capacitance at zero bias	[F/μm^2]	see p. 14
mje	B-E depletion capacitance exponent		see p. 14
Vje	B-E depletion capacitance diffusion voltage	[V]	see p. 14
Cjc	B-C depletion capacitance at zero bias	[F/μm^2]	see p. 14
mjc	B-C depletion capacitance exponent		see p. 14
Vjc	B-C depletion capacitance diffusion voltage	[V]	see p. 14
kjc	not used		
XJ0	Fraction of Cmin, lower limit of B-C capacitance		see p. 14
Cmin	minimum value of C_{bc}		see p. 14
	Extrinsic Parameters		
Rc	collector contact resistance	[Ω/finger]	see p. 5
Re	emitter contact resistance	[Ω/finger]	see p. 5
Rb	base contact resistance	[Ω/finger]	see p. 5
Rb2	base layer resistance	[Ω/finger]	see p. 5
Lc	extrinsic collector inductance not yet implemented in the Verilog version	[H]	see p. 5
Le	extrinsic emitter inductance not yet implemented in the Verilog version	[H]	see p. 5
Lb	extrinsic base inductance not yet implemented in the Verilog version	[H]	see p. 5
Cq	extrinsic C-B pad-capacitance	[F]	see p. 5
Cpb	base pad-capacitance	[F]	see p. 5
Cpc	collector pad-capacitance	[F]	see p. 5
	1/f Noise Parameters		
Kfb	base $1/f$ noise current source factor		see p. 16
Afb	base $1/f$ noise current source current exponent		see p. 16
Ffeb	base $1/f$ noise current source frequency exponent		see p. 16
Kb	base Lorentz noise current source factor		see p. 16
Ab	base Lorentz noise current source current exponent		see p. 16
Fb	base Lorentz noise current source time constant		see p. 16
Kfe	emitter noise voltage source factor		see p. 16

| Afe | emitter noise voltage source current exponent | see p. 16 |
| Ffee | emitter noise voltage source frequency exponent | see p. 16 |

References

[1] J. Hilsenbeck, F. Lenk, W. Heinrich, J. Würfl, "Low Phase Noise MMIC VCOs for Ka-Band Applications with Improved GaInP/GaAs-HBT Technology", *IEEE GaAs IC Symp. Dig.*, 2003, pp. 223 – 226.

[2] M. Rudolph, F. Lenk, R. Doerner, P. Heymann,
"Towards a Unified Method to Implement Transit-Time Effects in Pi-Topology HBT Compact Models"
in: IEEE MTT-S Int. Microwave Symp. Dig., 2002, 997-1000.

[3] M. Rudolph,
"Uniqueness Problems in Compact HBT Models Caused by Thermal Effects"
IEEE Trans. Microwave Theory Tech., vol. 52, 1399 – 1403, May 2004.

[4] J. C.-N. Huang, I. M. Abdel-Motaleb,
"Small-Signal Non-Quasi-Static Model for Single and Double Heterojunction Bipolar Transistors,"
Solid State Electron., vol. 36, pp. 1027 – 1034, July 1993.

[5] H. Klose, A. W. Wieder,
"The Transient Integral Charge Control Relation — A Novel Formulation of the Currents in a Bipolar Transistor,"
IEEE Trans. Electron Dev., vol. ED-34, pp. 1090 – 1099, May 1987.

[6] R. J. Whittier, D. A. Tremere,
"Current Gain and Cutoff Frequency Falloff at High Currents,"
IEEE Trans. Electron Dev., vol. ED-16, pp. 39 – 57, Jan. 1969.

[7] JCJ. Paasschens, W.J. Kloosterman, R. v.d. Toorn,
"Model derivation of MEXTRAM 504"
Koninklijke Philips Electronics N.V., Nat.Lab. Unclassified Report NL-UR 2002/806.

[8] M. Rudolph, R. Doerner, K. Beilenhoff, P. Heymann,
"Scalable GaInP/GaAs HBT Large-Signal Model"
IEEE Trans. Microwave Theory Tech., vol. 48, 2370 – 2376, Dec. 2000.

[9] C.-J. Wei, J. C. M. Hwang, W.-J. Ho, J. A. Higgins,
"Large-Signal Modeling of Self-Heating, Collector Transit-Time, and RF-Breakdown Effects in Power HBT's,"
IEEE Trans. Microwave Theory Tech., vol. 44, pp. 2641 – 2647, Dec. 1996.

[10] M. Rudolph, R. Doerner, K. Beilenhoff, P. Heymann,
"'Unified Model for Collector Charge in Heterojunction Bipolar Transistors'"
IEEE Trans. Microwave Theory Tech., vol. 50, 1747 – 1751, Juli 2002.

[11] M. Rudolph, R. Doerner, E. Richter, P. Heymann,
"Scaling of GaInP/GaAs HBT Equivalent-Circuit Elements"
in: GAAS 99 Dig., 1999, 113 – 116.

[12] M. Rudolph, R. Doerner, K. Beilenhoff, P. Heymann,
"Scalable GaInP/GaAs HBT Large-Signal Model"
in: IEEE MTT-S Int. Microwave Symp. Dig., 2000, 753 – 756.

[13] M. Rudolph, R. Doerner, L. Klapproth, P. Heymann,
      '"An HBT Noise Model Valid up to Transit Frequency"'
      IEEE Electron Dev. Lett., vol. 20, 24 – 26, Jan. 1999.

[14] P. Heymann, M. Rudolph, R. Doerner, F. Lenk,
      '"Modeling of Low-Frequency Noise in GaInP/GaAs Hetero-Bipolar-Transistors"'
      in: IEEE MTT-S Int. Microwave Symp. Dig., 2001, 1967 – 1970.

[15] M. Rudolph, R. Doerner, P. Heymann,
      "Direct Extraction of HBT Equivalent Circuit Elements"
      IEEE Trans. Microwave Theory Tech., vol. 47, 82 – 84, Jan. 1999.

[16] F. Lenk, M. Rudolph,
      "New Extraction Algorithm for GaAs-HBTs With Low Intrinsic Base Resistance"
      in: IEEE MTT-S Int. Microwave Symp. Dig., 2002, 725-728.

[17] N. Bovolon, P. Baureis, J.-E. Müller, P. Zwicknagl, R. Schultheis, E. Zanoni,
      "A Simple Method for the Thermal Resistance Measurement of AlGaAs/GaAs Hetero-
      junction Bipolar Transistors,"
      IEEE Trans. Electron Dev., vol. 45, pp. 1846 – 1848, Aug. 1998.

[18] M. Schröter, T.-Y. Lee,
      "Physics-Based Minority Charge and Transit Time Modeling for Bipolar Transistors,"
      IEEE Trans. Electron Dev., vol. 46, pp. 288 – 300, Feb. 1999.

A Equivalent Circuits and Names of Currents and Charges
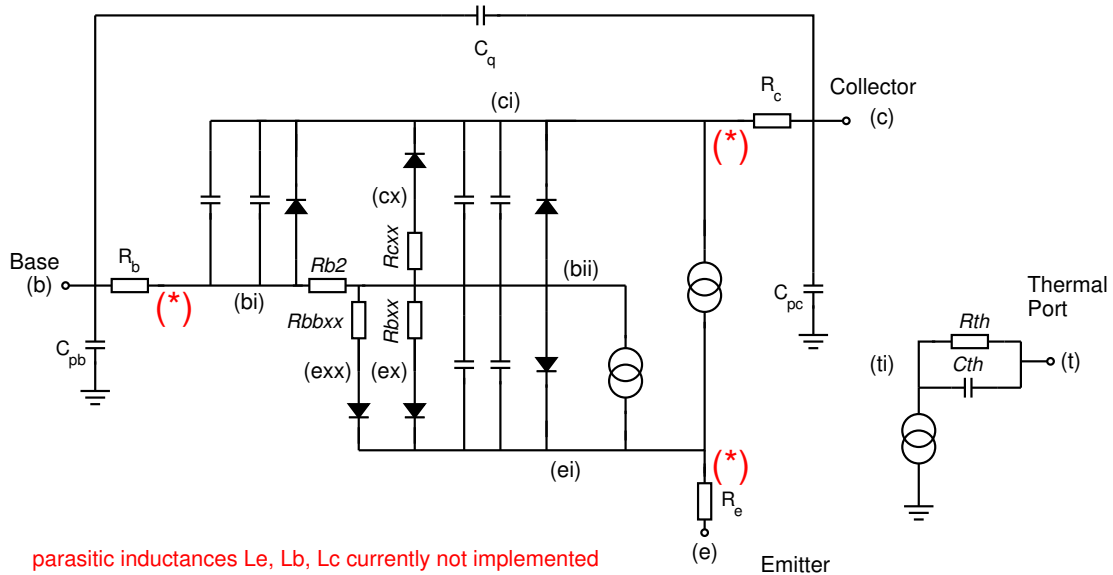
Linear Part of the Model and node names

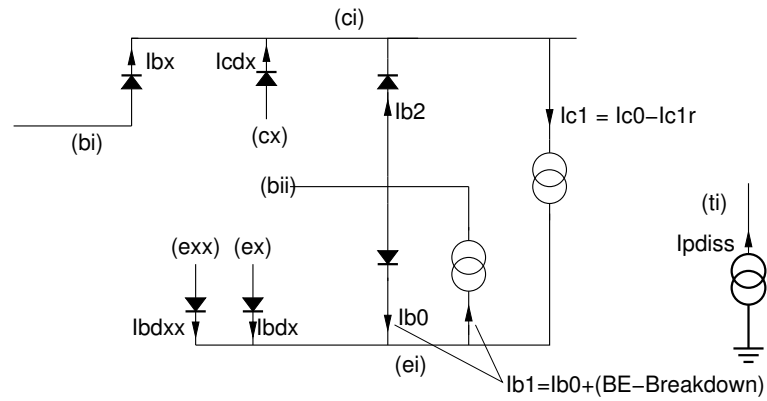Figure 14: Equivalent circuit with node names.

20

Names of current functions in the nonlinear model

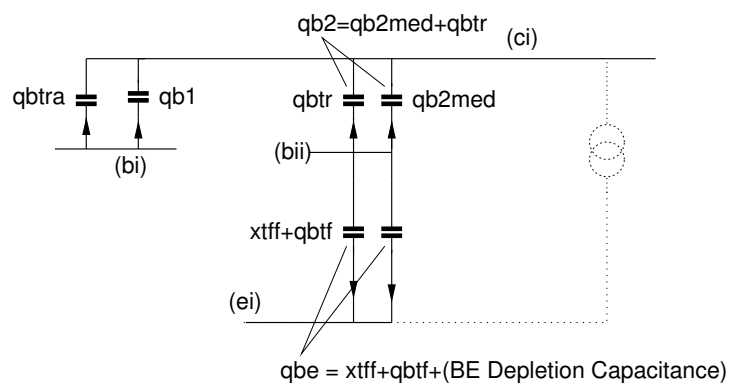Figure 15: Current sources of nonlinear subcircuit.

Names of charge functions in the nonlinear model

Figure 16: Charge sources of nonlinear subcircuit.